INTERNATIONAL JOURNAL FOR NUMERICAL METHODS IN FLUIDS
Int. J. Numer. Meth. Fluids 2006; **52**:571–590
Published online 14 February 2006 in Wiley InterScience (www.interscience.wiley.com). DOI: 10.1002/fld.1188

Runge–Kutta time-stepping schemes with TVD central differencing for the water hammer equations

E. M. Wahba*,†

Mechanical Engineering Department, Faculty of Engineering, Alexandria University, Alexandria 21544, Egypt

SUMMARY

In the present study, Runge–Kutta schemes are used to simulate unsteady flow in elastic pipes due to sudden valve closure. The spatial derivatives are discretized using a central difference scheme. Second-order dissipative terms are added in regions of high gradients while they are switched off in smooth flow regions using a total variation diminishing (TVD) switch. The method is applied to both one- and two-dimensional water hammer formulations. Both laminar and turbulent flow cases are simulated. Different turbulence models are tested including the Baldwin–Lomax and Cebeci–Smith models. The results of the present method are in good agreement with analytical results and with experimental data available in the literature. The two-dimensional model is shown to predict more accurately the frictional damping of the pressure transient. Moreover, through order of magnitude and dimensional analysis, a non-dimensional parameter is identified that controls the damping of pressure transients in elastic pipes.

KEY WORDS: water hammer; Runge–Kutta scheme; unsteady friction

1. INTRODUCTION

The term ‘water hammer’ is used to describe unsteady flow in pipes, which is generally caused by sudden or rapid changes in flow conditions. These changes could occur due to sudden valve closure, pump start up or shut down, etc. This problem is of great practical importance, as it could ultimately damage the entire piping system. A detailed review of water hammer theory and practice is given by Ghidaoui *et al.* [1].

One-dimensional (1-D) models are available for unsteady flow in pipes, which are based on the conservation of mass and axial momentum. Pipe elasticity is included in the model through the expression for the wave speed. The unknown variables are the pressure head and

*Correspondence to: E. M. Wahba, Mechanical Engineering Department, Faculty of Engineering, Alexandria University, Alexandria 21544, Egypt.
†E-mail: emwahba@yahoo.com

Received 1 November 2005
Revised 9 December 2005
Accepted 26 December 2005

the average velocity at each cross section. The equations of conservation of mass and axial momentum form a (2×2) hyperbolic system that can be elegantly solved using the method of characteristics (MOC). More details about the implementation of the MOC to the water hammer problem can be found in Reference [2].

Other methods of solution for the 1-D model include implicit methods [3], Godunov methods [4] and finite element methods [5]. However, MOC still remains the method of choice for the 1-D problem.

The 1-D model provides an excellent prediction of the magnitude of the first pressure peak. On the contrary, it underestimates the attenuation of the following pressure peaks resulting in much higher simulated pressure values than those experimentally observed. The reason for this is due to the inadequate representation of the frictional damping mechanism in the 1-D model. Viscous damping is introduced in the model through a quasi-steady representation, which evaluates the instantaneous shear stress by the value that would occur at the same average velocity in steady flow. Although this approximation gives good results for relatively slow transients, it performs poorly in case of fast transients. The main problem of the quasi-steady representation is that it assumes that the velocity profile in unsteady flow would be similar to that in steady flow, which is not the case for fast transients in which strong adverse pressure gradients could result in large regions of flow separation and reversal in the pipe.

Improvements to the quasi-steady approximation of the 1-D model were proposed by several authors, such as in the work by Zielke [6], Brunone *et al.* [7–9] and Vardy *et al.* [10–12]. These modifications resulted in significant improvements in the modelling of the attenuation of the pressure peaks and showed that the 1-D assumption is an invalid assumption for fast transients in pipes. Therefore, two-dimensional (2-D) models should be considered if accurate simulations of fast transients are required, and if it is desired to understand how the velocity profile behaves under transient conditions.

A rather limited number of simulations for the 2-D problem of unsteady flow in elastic pipes due to rapid transients are available in the literature [13–17]. In the 2-D model, the 2-D form of the axial momentum equation is retained where the local velocity is now a function of both the axial and radial directions together with being a function of time. Several schemes were used to solve the governing equations such as the explicit predictor–corrector methods or the implicit methods. In Reference [16], turbulence modelling was included through a simple two-zone model based on the mixing length hypothesis in the turbulent core and on Newton's law in the viscous sublayer. However, it was reported that explicit predictor–corrector schemes suffered from stability limitations, while implicit schemes resulted in more laborious computations.

The purpose of the present work is to introduce a method that solves both 1-D and 2-D models using a fourth-order Runge–Kutta time-stepping scheme in order to extend the stability region of the unsteady flow solver. Also, numerical oscillations are prevented through the use of second-order dissipative terms that are added in regions of high gradients and are switched off in smooth regions by using a switch that is total variation diminishing (TVD). Moreover, alternative turbulence models are tested in the present study through the use of the Baldwin–Lomax model [18] and the Cebeci–Smith model [19] in order to examine their ability to simulate fast transients in piping systems. Finally, the non-dimensional parameter controlling the viscous effects, and hence the damping of the pressure peaks, in unsteady pipe flow is identified.

2. NUMERICAL METHODS FOR 1-D UNSTEADY PIPE FLOW MODEL

The governing equations for the 1-D model, in matrix form, are:

$$\frac{\partial W}{\partial t} + B\frac{\partial W}{\partial x} = C$$
$$W = \begin{bmatrix} H \\ V \end{bmatrix} \quad B = \begin{bmatrix} V & \frac{a^2}{g} \\ g & V \end{bmatrix} \quad C = \begin{bmatrix} 0 \\ -\frac{fV|V|}{2D} \end{bmatrix} \tag{1}$$

The system is hyperbolic with the slope of the characteristic lines given by $(V \pm a)$. The quasi-steady approximation for the viscous term is employed, where the value of the friction factor (f) is obtained from the instantaneous value of the average velocity at the cross section using the steady state relations.

A fourth-order Runge–Kutta scheme is used to integrate the system of equations in time. Spatial derivatives are discretized using second-order central difference expressions. Second-order dissipative terms, similar to those introduced by Jameson *et al.* [20], are added to the equations in regions of high gradients to eliminate numerical oscillations. The dissipative terms are effectively switched off in smooth flow regions. After adding the dissipative terms, the system of Equations (1) can be re-written in the following form:

$$\frac{\partial W}{\partial t} + B\frac{\partial W}{\partial x} = C + A_v(W) \tag{2}$$

(A_v) represents the dissipative operator which is defined as follows:

$$A_v(W) = \frac{1}{\Delta t}[\varepsilon_{i+1/2}(W_{i+1} - W_i) - \varepsilon_{i-1/2}(W_i - W_{i-1})]$$
$$\varepsilon_{i+1/2} = \tfrac{1}{2}\max(\alpha_{i+2}, \alpha_{i+1}, \alpha_i, \alpha_{i-1}) \tag{3}$$

where the index i denotes spatial location. In their numerical scheme, Jameson *et al.* [20] use a blend of second- and fourth-order dissipative terms for the Euler equations. The fourth-order terms are added to allow the calculations to converge to a completely steady state. Hence, for unsteady problems as the one considered in the present study, there is no need for such fourth-order terms. The numerical switch (α) represents a switch for detecting regions of high gradients. Different switches could be used. In the present paper, the TVD switch introduced by Swanson and Turkel [21] is applied.

$$\alpha_i = \frac{|W_{i+1} - 2W_i + W_{i-1}|}{(1-\omega)\Psi_{\text{TVD}} + \omega\Psi}$$
$$\Psi_{\text{TVD}} = |W_{i+1} - W_i| + |W_i - W_{i-1}|, \quad \Psi = |W_{i+1} + 2W_i + W_{i-1}| \tag{4}$$

and $0 \leqslant \omega \leqslant 1$. The TVD condition is attained at $(\omega \ll 1)$. To provide some insight about the performance of the TVD switch (α), it is useful to re-write Equation (4), with $(\omega = 0)$, in

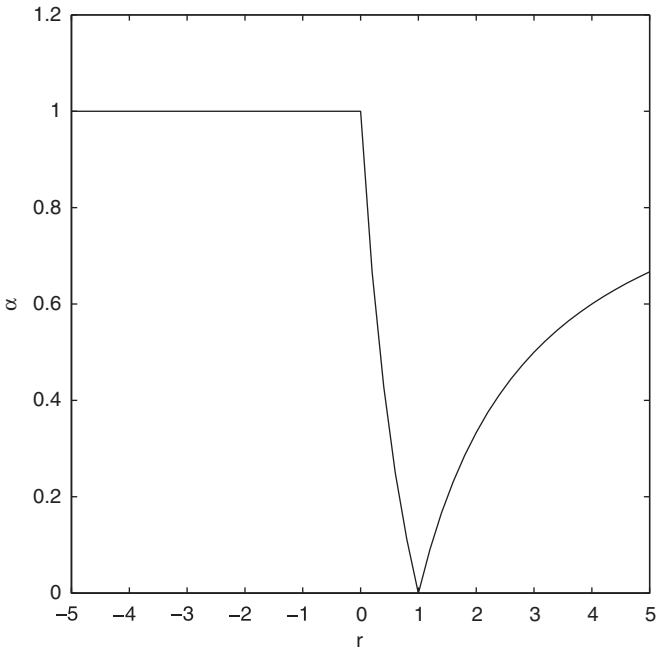

Figure 1. TVD switch performance as a function of (r).

the following form:

$$\alpha_i = \frac{|1-r|}{1+r} = \begin{cases} \dfrac{|1-r|}{1+r} & r>0 \\ 1 & r\leqslant 0 \end{cases} \qquad r = \frac{W_i - W_{i-1}}{W_{i+1} - W_i} \tag{5}$$

Equation (5) is plotted in Figure 1. For smooth flow regions ($r = 1$), the value of (α) is zero and hence the dissipative terms are switched off. Otherwise, for regions of high gradients, (α) has a positive value with an upper limit of ($\alpha = 1$) and dissipation is added in these regions.

3. NUMERICAL METHODS FOR 2-D UNSTEADY PIPE FLOW MODEL

For 2-D axi-symmetric unsteady flow, the Navier–Stokes equations can be written in the form

$$\begin{aligned} &\frac{\partial \rho}{\partial t} + \frac{\partial(\rho u)}{\partial x} + \frac{1}{r}\frac{\partial(\rho r v)}{\partial r} = 0 \\ &\frac{\partial u}{\partial t} + u\frac{\partial u}{\partial x} + v\frac{\partial u}{\partial r} = -g\frac{\partial H}{\partial x} + \frac{1}{\rho}\frac{\partial \tau_{xx}}{\partial x} + \frac{1}{\rho r}\frac{\partial(r\tau_{rx})}{\partial r} \\ &\frac{\partial v}{\partial t} + u\frac{\partial v}{\partial x} + v\frac{\partial v}{\partial r} = -g\frac{\partial H}{\partial r} + \frac{1}{\rho}\frac{\partial \tau_{xr}}{\partial x} + \frac{1}{\rho r}\frac{\partial(r\tau_{rr})}{\partial r} - \frac{\tau_{\theta\theta}}{\rho r} \end{aligned} \tag{6}$$

Some common approximations are used to simplify this set of equations for the case of unsteady flow in elastic pipes. The first approximation is to replace the radial momentum equation by its boundary layer theory counterpart

$$\frac{\partial H}{\partial r} = 0 \tag{7}$$

In other words, the pressure head (H) is a function of (x) and (t) only. Mass conservation is integrated over the whole cross section resulting in

$$\frac{\partial H}{\partial t} + V\frac{\partial H}{\partial x} + \frac{a^2}{g}\frac{\partial V}{\partial x} = 0 \tag{8}$$

Moreover, the flow is assumed to be one-directional. Hence, the axial momentum equation takes the simplified form

$$\frac{\partial u}{\partial t} + u\frac{\partial u}{\partial x} = -g\frac{\partial H}{\partial x} + \frac{1}{\rho r}\frac{\partial(r\tau_{rx})}{\partial r} \tag{9}$$

The shear stress term (τ_{rx}) is evaluated from

$$\tau_{rx} = \rho(\nu + \nu_t)\frac{\partial u}{\partial r} \tag{10}$$

where (ν_t) is the eddy viscosity, which is zero for laminar flows and evaluated using a suitable turbulence model for turbulent flows. In the present study, two turbulence models are used to examine their effectiveness in simulating transient turbulent pipe flow. The tested turbulence models are the Baldwin–Lomax model [18] and the Cebeci–Smith model [19]. A detailed explanation of both models is given in Appendix A.

A numerical scheme similar to that applied to the 1-D model is used to solve the 2-D model. The fourth-order Runge–Kutta scheme is used to integrate the mass and axial momentum equations in time, central differencing is used to approximate the spatial derivatives and second-order dissipative terms are switched on in regions of high gradients using the TVD switch. The average velocity (V) is evaluated from the local velocity (u) at each cross section using the formula

$$V = \frac{\int_0^R u 2\pi r\,\mathrm{d}r}{\pi R^2} \tag{11}$$

In the following section, numerical results of the (1-D) and (2-D) models are presented and compared to analytical results and to experimental data available in the literature.

4. NUMERICAL RESULTS

Numerical results for a reservoir–pipe–valve configuration are presented. The first simulation is an inviscid 1-D simulation due to sudden valve closure. The pipe is divided into 200 parts with CFL = 1. This case represents an extreme case with a steep pressure front propagating in the pipe indefinitely. The case provides a good test for the numerical model, especially in terms of examining the numerical dissipation and dispersion aspects of the model.

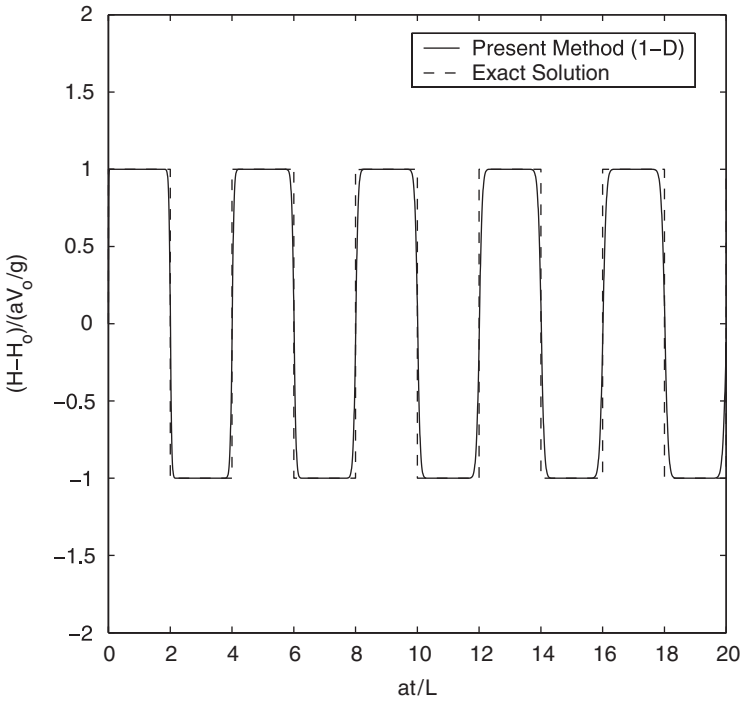

Figure 2. Pressure–time history at the valve (1-D simulation, inviscid case).

The exact solution of the problem is known when the convective acceleration terms are neglected, hence $V = 0$ in matrix B. This solution is represented by a pressure–time history at the valve in the form of a square wave. A comparison between the results of the present method and the exact solution is given in Figure 2. The dissipative terms, together with the TVD switch, eliminate any numerical oscillations resulting in a monotonic behaviour as evident from Figure 2. Numerical dissipation is also minimized resulting in sharp pressure fronts, which keep their integrity over a long time. To demonstrate the effectiveness of the TVD switch and the dissipative terms, the test case is re-simulated with no dissipative terms (the switch α is set to zero at all spatial nodes). The results of this simulation are given in Figure 3, which shows significant dispersive errors, which contaminate the numerical solution.

The 1-D and 2-D models are used to simulate unsteady flow in the reservoir–pipe–valve system of Holmboe and Rouleau [22], for which both laminar and turbulent flow experimental data exist. The pipe has an inner diameter of 0.025 m, a length of 36.09 m and is made of copper. Pressure signals directly upstream of the valve and at the pipe midpoint are recorded. The operating fluid in the laminar flow case (Reynolds number $= 82$) is high-viscosity oil ($\mu = 0.03484\,\mathrm{N\,s/m^2}$) and the wave speed is measured to be 1324 m/s. For the turbulent flow case (Reynolds number $= 6166$), the operating fluid is water with a wave speed of 1350 m/s.

The 1-D model is used to simulate the laminar flow case. The pipe is divided into 200 parts with CFL $= 1$. The results of the simulation are given in Figures 4 and 5. The 1-D model clearly underestimates the viscous damping of the pressure transient.

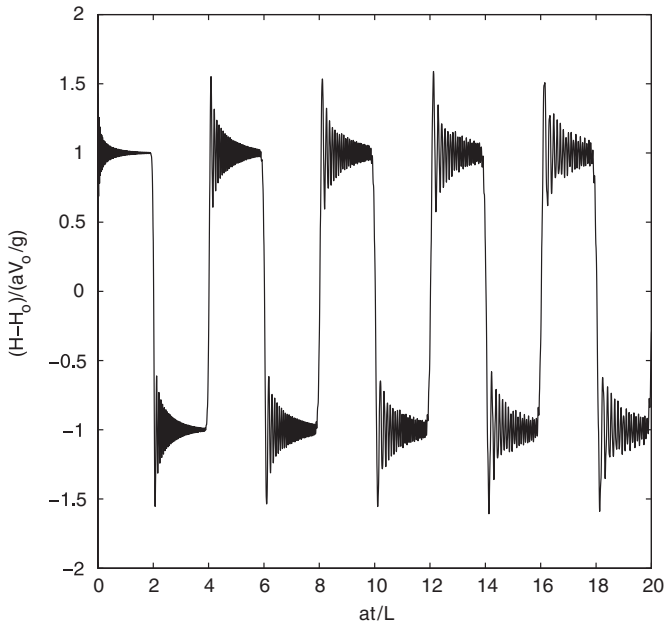

Figure 3. Pressure–time history at the valve (1-D simulation, inviscid case, no dissipation).

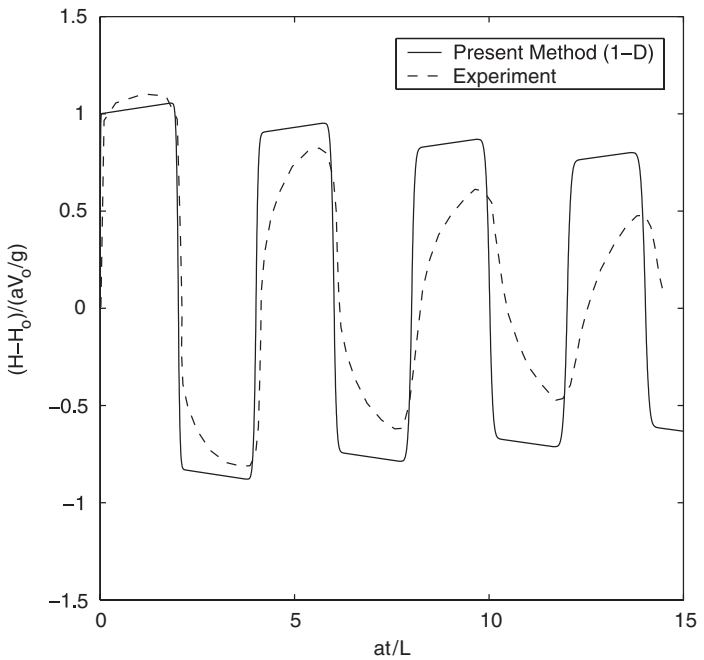

Figure 4. Pressure–time history at the valve (1-D simulation, laminar flow, $Re = 82$).

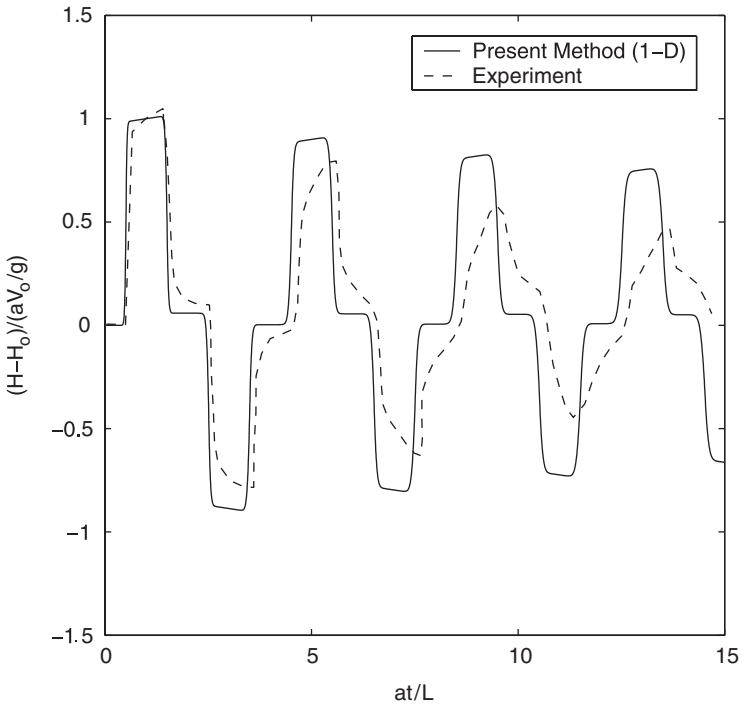

Figure 5. Pressure–time history at the midpoint (1-D simulation, laminar flow, $Re = 82$).

Simulations using the 2-D model are performed. The pipe is discretized using 200 parts in the axial direction and 60 parts in the radial direction with CFL = 1. Comparisons between the simulated pressure transients and the experimentally recorded ones at the valve and midpoint, for the laminar flow case ($\nu_t = 0$), are given in Figures 6 and 7, respectively. The results confirm that the attenuation of the pressure peaks could be efficiently recovered using the 2-D model. Further insight could be provided through monitoring the evolution of the velocity profile during the transient. The velocity profile at the midpoint is plotted in Figure 8 at various time instants. Figure 8 shows velocity profiles that differ significantly from the steady state parabolic profile, hence further confirming the inadequacy of using the quasi-steady approximation for the viscous term. In fact, at more than one time instant, the flow in the neighbourhood of the pipe wall is in reverse direction with respect to the average velocity at the cross section, which means that the wall shear stress and the average velocity are not even in phase.

The turbulent flow case is simulated next. The pipe is discretized using 200 parts in the axial direction and 160 parts in the radial direction with CFL = 0.5. Both the Baldwin–Lomax [18] and Cebeci–Smith [19] models are used to compute the Reynolds stress term via the Boussinesq approximation.

The steady state turbulent velocity profile is needed as an initial condition for the unsteady flow computations. For fully developed steady pipe flow, the shear stress achieves its largest value at the pipe wall (τ_w) and decreases linearly to zero at the pipe centreline.

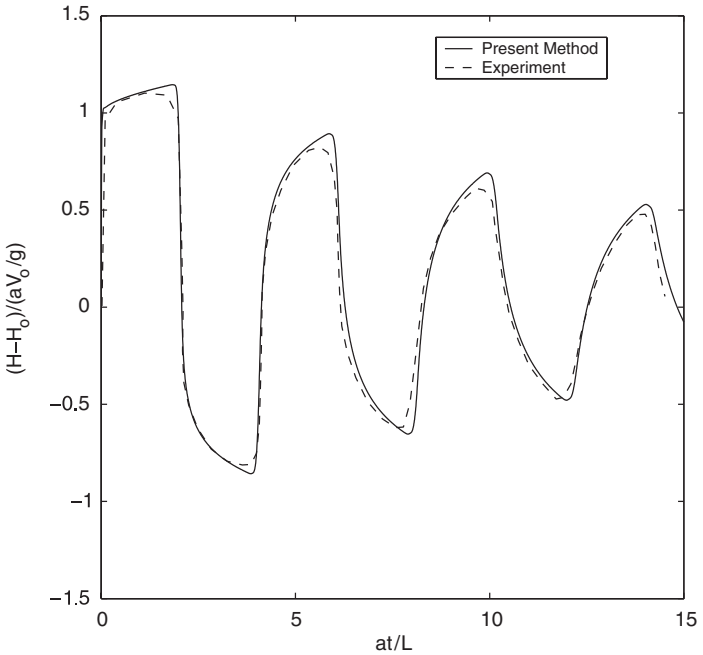

Figure 6. Pressure–time history at the valve (2-D simulation, laminar flow, $Re = 82$).

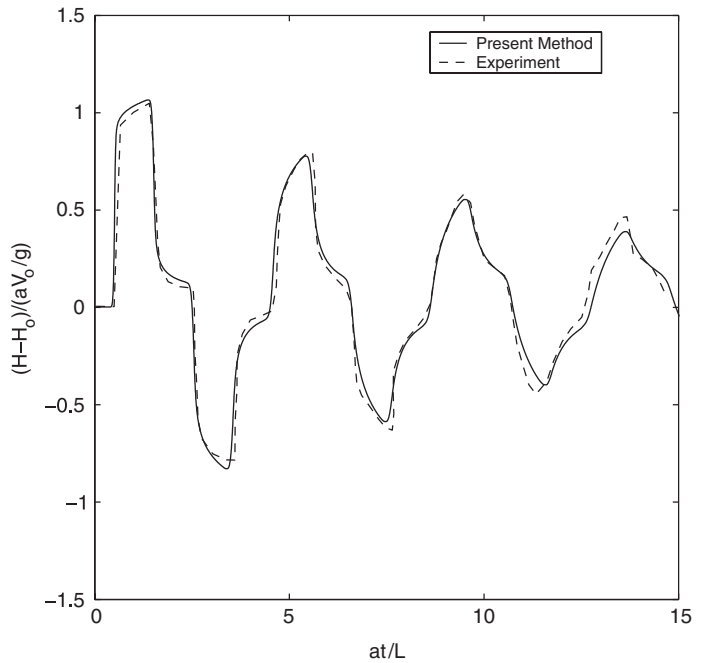

Figure 7. Pressure–time history at the midpoint (2-D simulation, laminar flow, $Re = 82$).

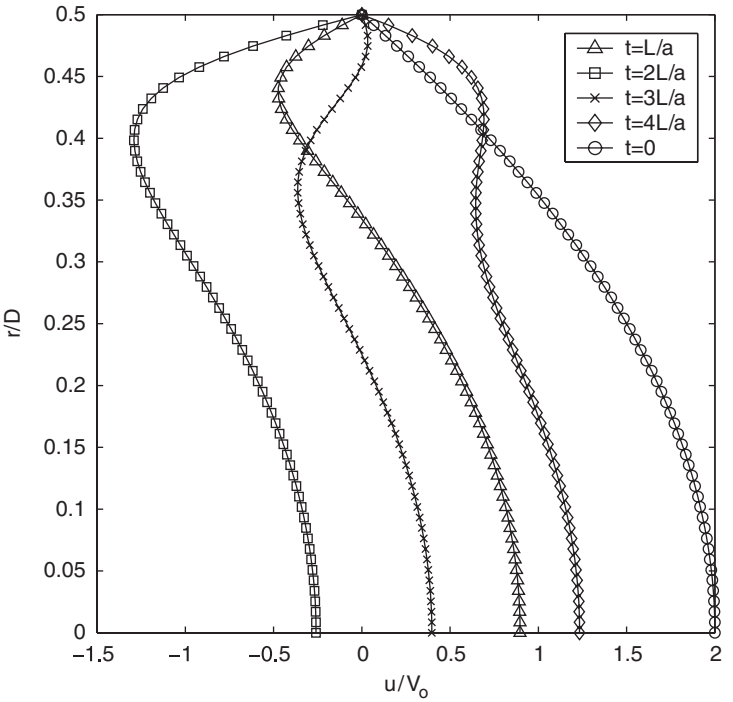

Figure 8. Velocity profiles at the midpoint at different times (2-D simulation, laminar flow, $Re = 82$).

Hence, Equation (10) can be re-written in the following form:

$$\frac{\tau_{rx}}{\rho} = (v + v_t)\frac{\partial u}{\partial y} = u_\tau^2 \left(1 - \frac{y}{R}\right) \tag{12}$$

where $u_\tau = \sqrt{\tau_w/\rho}$ is the friction velocity. Following Wilcox [23], Equation (12) is integrated using the trapezoidal rule to obtain the velocity profile, while the eddy viscosity (v_t) is evaluated from the turbulence model. It should be noted that for the Cebeci–Smith model, the velocity thickness δ_v^* is not known until the entire velocity profile is determined. Similarly, for the Baldwin–Lomax model, the value of $y_{\max}$ is not known until the entire velocity profile is determined. Hence, an iterative procedure is required in order to obtain the steady state turbulent velocity profile.

An initial assumption for (u_τ) is needed to start the computation. A good initial assumption could be obtained from the friction factor (f) obtained from Prandtl's universal law of friction for smooth pipes at the desired Reynolds number

$$\frac{1}{\sqrt{f}} = 2\,\log(Re\sqrt{f}) - 0.8$$

$$u_\tau = \sqrt{\frac{fV^2}{8}}$$

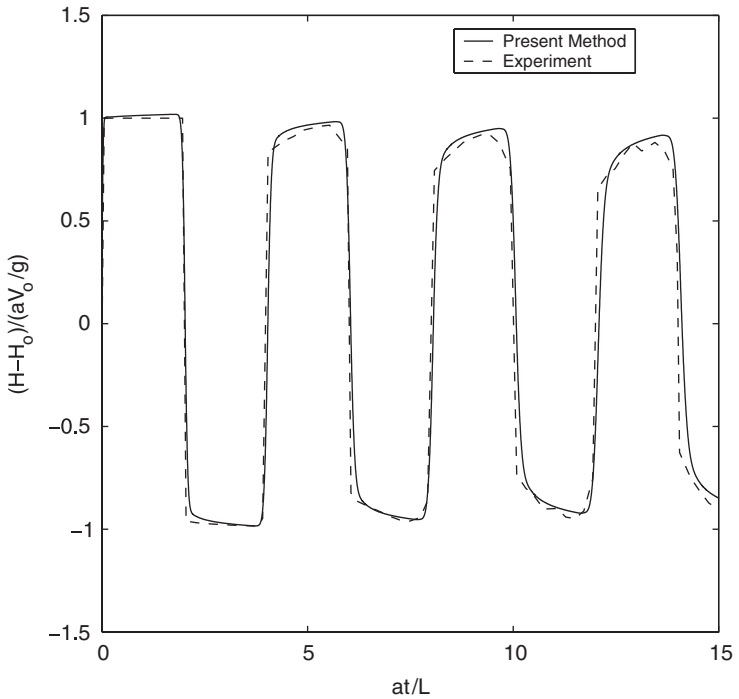

Figure 9. Pressure–time history at the valve (2-D simulation, Baldwin–Lomax model, $Re = 6166$).

However, it was shown by Wilcox [23] that for the same Reynolds number, computed (u_τ) values using the Baldwin–Lomax and Cebeci–Smith models differ by about 1–7% from the values predicted by Prandtl's formula. Hence, a shooting procedure is adopted in order to find the right value for (u_τ) needed by the turbulence model to obtain the desired flow rate.

Unsteady turbulent flow simulations using the Baldwin–Lomax model [18] are given in Figures 9 and 10, while those for the Cebeci–Smith model [19] are given in Figures 11 and 12. Comparisons with the experimental pressure transient recordings at the valve and midpoint indicate that both turbulence models perform equally well in predicting the pressure transient for unsteady turbulent pipe flow.

For the sake of completeness, the turbulent flow case is re-simulated using the 1-D model. The results of the 1-D simulation are compared with the 2-D results obtained using the Baldwin–Lomax model in Figure 13 at the valve. As seen from Figure 13, the effect of the 2-D turbulence modelling is relatively small, unlike the laminar flow case in which the 2-D modelling had a profound effect. Combining the previous statement with the fact that numerical and experimental uncertainties could possibly have a larger effect than the 2-D turbulence modelling effect, one should approach the good agreement shown in Figures 9 and 10 with caution. On the other hand, the ability of the 2-D turbulence model to effectively capture the rounding of the pressure peaks, which was completely missed by the 1-D model, should provide more confidence in the quality of the 2-D turbulence modelling. At any rate, more experimental unsteady turbulent flow data are needed for further validation of the 2-D unsteady turbulent flow modelling.

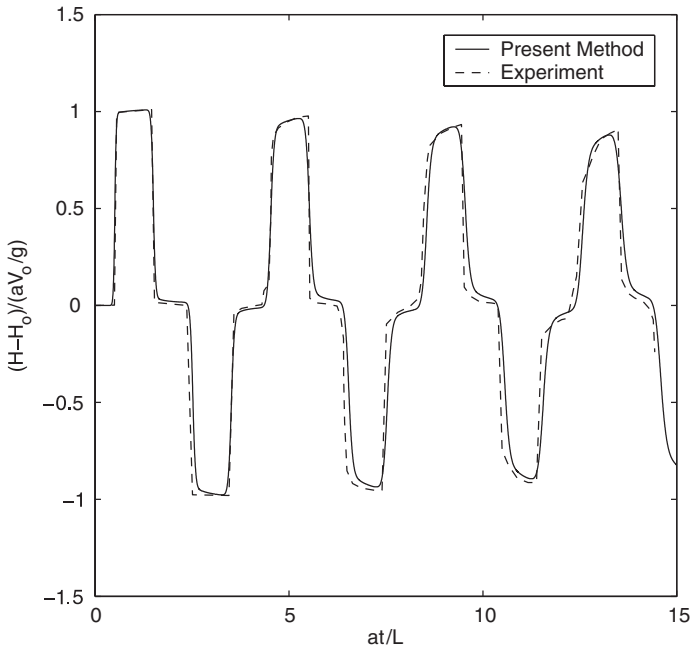

Figure 10. Pressure–time history at the midpoint (2-D simulation, Baldwin–Lomax model, $Re = 6166$).

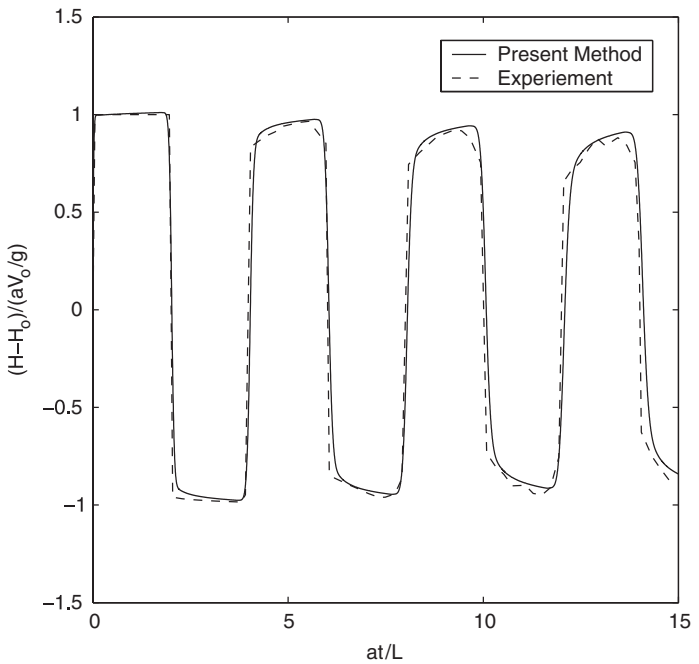

Figure 11. Pressure–time history at the valve (2-D simulation, Cebeci–Smith model, $Re = 6166$).

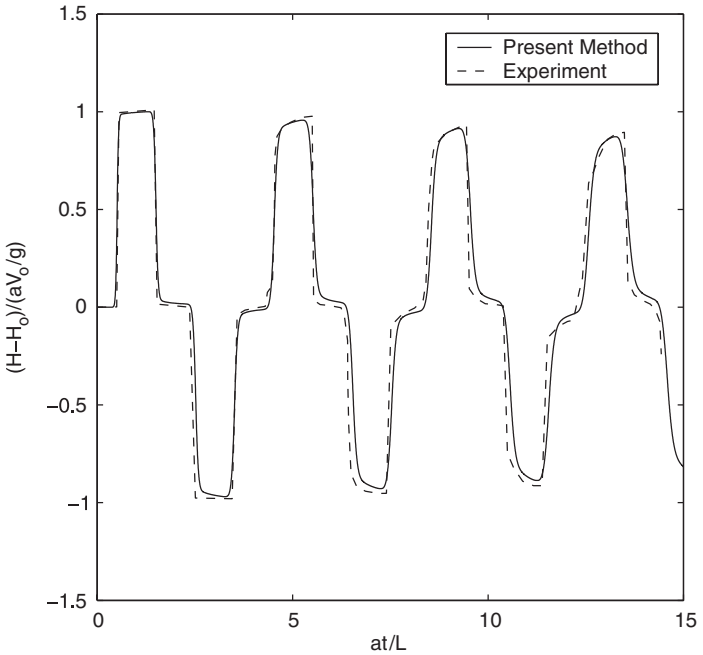

Figure 12. Pressure–time history at the midpoint (2-D simulation, Cebeci–Smith model, $Re = 6166$).

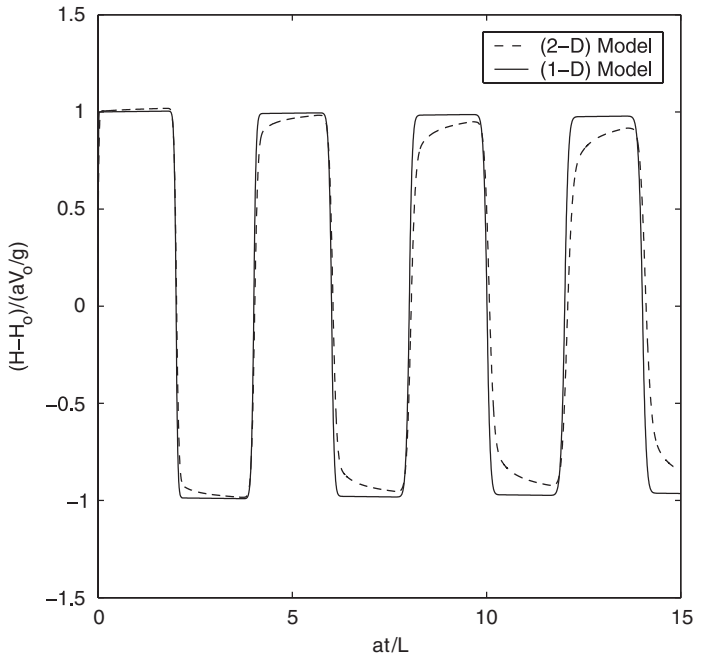

Figure 13. One- and two-dimensional simulations at the valve (Baldwin–Lomax model, $Re = 6166$).

5. NON-DIMENSIONAL PARAMETER FOR VISCOUS EFFECTS IN UNSTEADY PIPE FLOW

Further investigation of the unsteady friction damping mechanism is undergone in the present section. The laminar test case ($Re = 82$) is re-simulated using water as the operating fluid. The Reynolds number is kept constant and equal to 82 by changing the steady state velocity in the pipe. The same discretization is used as in the oil case, where the pipe is divided into 200 parts in the axial direction and 60 parts in the radial direction with CFL = 1. The simulated pressure transients with water as the operating fluid are compared with those of oil as the operating fluid in Figures 14 and 15. Although both cases have the same Reynolds number, the unsteady frictional effects are much stronger for oil than water. This rather surprising result warrants a careful order of magnitude analysis of the axial momentum equation in order to reveal the non-dimensional parameter governing viscous effects in unsteady pipe flow.

Starting with Equation (9), the different variables are normalized according to the following relations:

$$u^* = \frac{u}{V_0}, \quad H^* = \frac{H}{aV_0/g}, \quad r^* = \frac{r}{D}, \quad t^* = \frac{t}{L/a}, \quad x^* = \frac{x}{L}$$

Note that the characteristic time scale is now of order (L/a) and not (L/V_0), while the pressure head is of order (aV_0/g). Substituting into the axial momentum equation (9) and taking

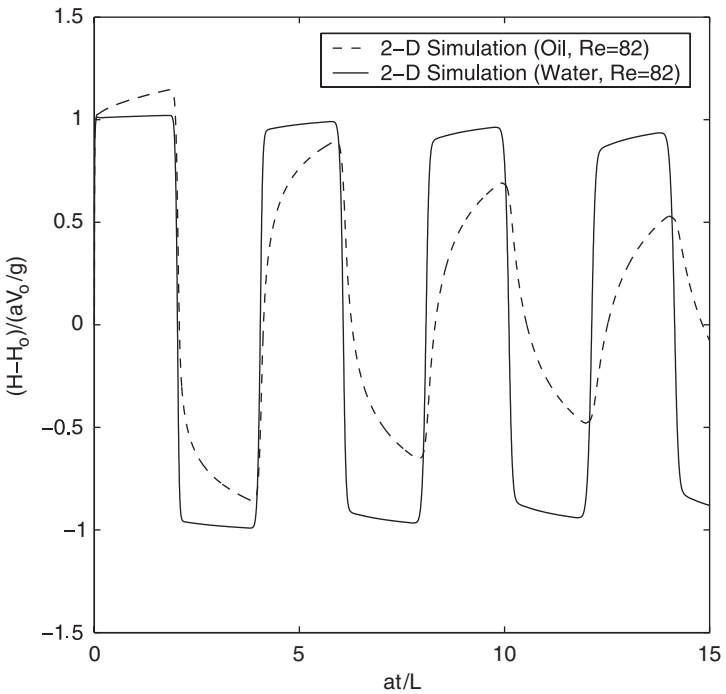

Figure 14. Pressure–time history at the valve for different liquids (2-D simulation, $Re = 82$).

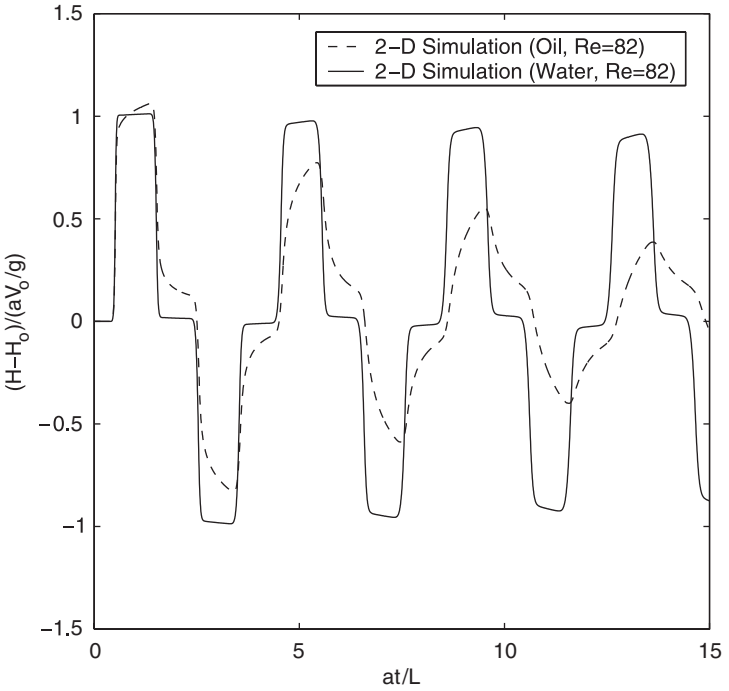

Figure 15. Pressure–time history at the midpoint for different liquids (2-D simulation, $Re = 82$).

($v_t = 0$), without any loss of generality, the non-dimensionalized axial momentum equation takes the form

$$\frac{\partial u^*}{\partial t^*} + \left(\frac{V_0}{a}\right) u^* \frac{\partial u^*}{\partial x^*} = -\frac{\partial H^*}{\partial x^*} + \left(\frac{Lv}{aD^2}\right) \frac{1}{r^*} \frac{\partial \left(r^* \dfrac{\partial u^*}{\partial r^*}\right)}{\partial r^*} \tag{13}$$

From Equation (13), it is clear that the convective acceleration is negligible with respect to the temporal acceleration for low Mach number flows. The non-dimensional parameter (aD^2/Lv) is shown to control the viscous term instead of Reynolds number. It shows that unsteady viscous effects are much stronger in longer pipes of smaller diameters, and in highly viscous fluids of smaller wave speeds. To demonstrate the validity of the above analysis, the numerical simulation with water as the operating fluid is repeated, but this time with fixing the non-dimensional parameter (aD^2/Lv) equal to the oil flow case. A comparison of the results of the water and oil simulations is given in Figures 16 and 17 demonstrating, numerically, that unsteady viscous effects are, in fact, governed by the non-dimensional parameter (aD^2/Lv).

The non-dimensional parameter (aD^2/Lv) could be identified through an alternative approach. In an illuminating paper by Sir George Gabriel Stokes [24], it was shown that the hydrodynamic resistance affecting the motion of a pendulum in a fluid is dependent on the non-dimensional parameter (D^2/vT), where T represents the periodic time. The importance of this parameter was realized in numerous flow problems such as oscillatory separated flows over bluff bodies. A recent summary regarding this non-dimensional parameter is

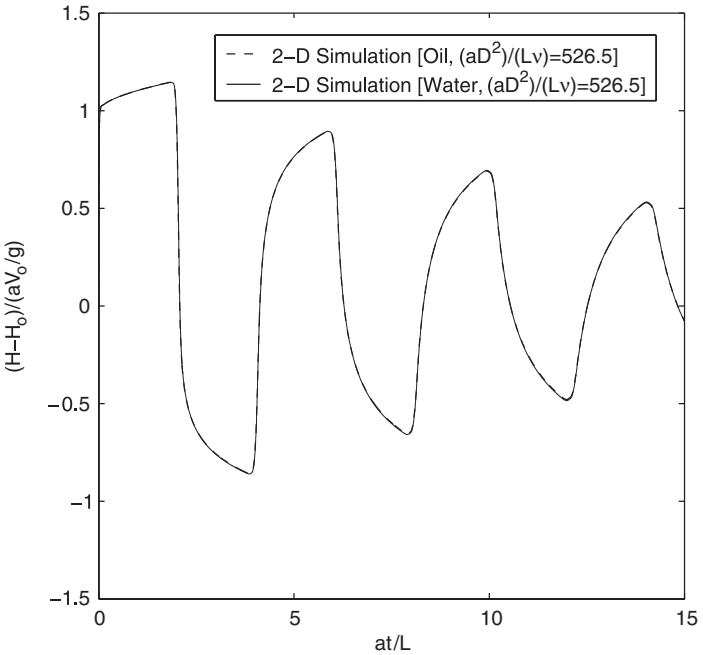

Figure 16. Pressure–time history at the valve for different liquids (2-D simulation, $aD^2/Lv = 526.5$).

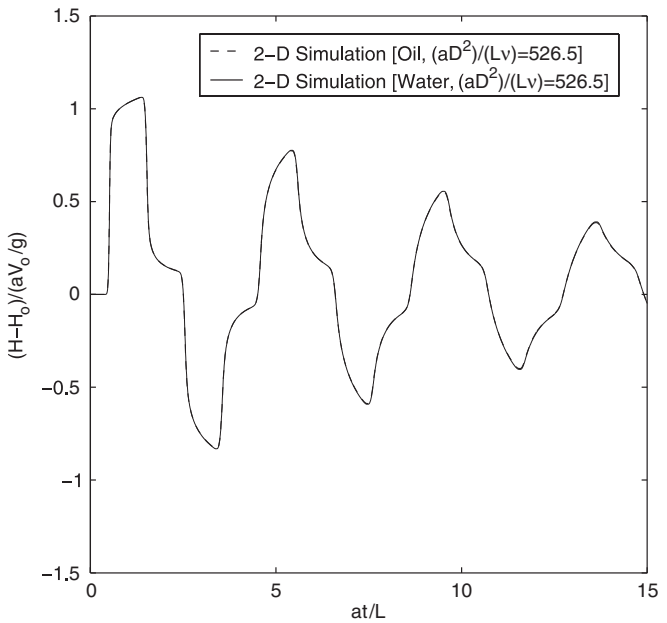

Figure 17. Pressure–time history at the midpoint for different liquids (2-D simulation, $aD^2/Lv = 526.5$).

given by Sarpkaya [25]. This parameter could be effectively extended to the present problem, which is concerned with viscous effects in unsteady pipe flow, by noting that the periodic time for unsteady flows in elastic pipes is of the order (L/a). Hence, replacing $(T = L/a)$ into the non-dimensional parameter $(D^2/\nu T)$ results in $(aD^2/L\nu)$, which is the same non-dimensional parameter obtained from the order of magnitude analysis and verified using numerical experiments.

6. CONCLUSIONS

A fourth-order Runge–Kutta scheme is developed and used to simulate unsteady flow in elastic pipes due to sudden valve closure. Both one- and two-dimensional formulations of the problem are considered. Spatial derivatives are discretized using a central difference scheme. Second-order dissipative terms are added in regions of high gradients to prevent numerical oscillations while they are switched off in smooth flow regions using a TVD switch. Both laminar and turbulent flow cases are simulated. Different turbulence models are tested including the Baldwin–Lomax and Cebeci–Smith models. The results of the present method are in good agreement with analytical solutions and experimental data available in the literature. The two-dimensional model is shown to successfully simulate the attenuation of the pressure peaks during the transient. Moreover, through order of magnitude and dimensional analysis, a non-dimensional parameter is identified that controls the viscous effect in unsteady pipe flow.

APPENDIX A: TURBULENCE MODELS

Two turbulence models are used in the present study, namely the Cebeci–Smith and the Baldwin–Lomax models. The Cebeci–Smith model is a two-layer algebraic turbulence model, with the eddy viscosity (ν_t) given by separate expressions in each layer

$$\nu_t = \begin{cases} \nu_{t_i} & y \leqslant y_m \\ \nu_{t_o} & y > y_m \end{cases} \tag{A1}$$

where y_m is the smallest value of y for which $\nu_{t_i} = \nu_{t_o}$. The values of the eddy viscosity in the inner layer, ν_{t_i}, and the outer layer, ν_{t_o}, are evaluated from the following expressions:

$$\nu_{t_i} = l_{\text{mix}}^2 \left| \frac{\partial u}{\partial y} \right|$$

$$l_{\text{mix}} = \kappa y [1 - \mathrm{e}^{-y^+/26}]$$

$$\nu_{t_o} = \beta U_e \delta_v^* F_{\text{Kleb}}(y; \delta)$$

where y^+ is the dimensionless sublayer-scaled distance $(u_\tau y/\nu)$. The following closure coefficients are used for the Cebeci–Smith model:

$$\kappa = 0.4, \quad \beta = 0.0168$$

The function F_{Kleb} is the Klebanoff intermittency function given by

$$F_{\text{Kleb}}(y;\delta) = \left[1 + 5.5\left(\frac{y}{\delta}\right)^6\right]^{-1}$$

where δ is the boundary layer thickness, U_e is the boundary layer edge velocity and δ_v^* is the velocity thickness defined by

$$\delta_v^* = \int_0^\delta \left(1 - \frac{u}{U_e}\right) \mathrm{d}y$$

The Baldwin–Lomax model is also a two-layer algebraic turbulence model in which the eddy viscosity (ν_t) is again given by Equation (A1). The expressions for the eddy viscosity in the inner and outer layers are

$$\nu_{t_i} = l_{\text{mix}}^2 \left|\frac{\partial u}{\partial y}\right|$$

$$l_{\text{mix}} = \kappa y[1 - \mathrm{e}^{-y^+/26}]$$

$$\nu_{t_o} = \beta C_{\text{cp}} F_{\text{wake}} F_{\text{Kleb}}(y; y_{\max}/C_{\text{Kleb}})$$

$$F_{\text{wake}} = \min(y_{\max} F_{\max}; C_{\text{wk}} y_{\max} U_{\text{dif}}^2 / F_{\max})$$

$$F_{\max} = \frac{1}{\kappa}\left[\max_y\left(l_{\text{mix}}\left|\frac{\partial u}{\partial y}\right|\right)\right]$$

$$U_{\text{dif}} = |u|_{\max} - |u|_{y=y_{\max}}$$

where $y_{\max}$ is the value of y at which $l_{\text{mix}}|\partial u/\partial y|$ attains its maximum value. The closure coefficients for the Baldwin–Lomax model are

$$\kappa = 0.4, \quad \beta = 0.0168, \quad C_{\text{cp}} = 1.6, \quad C_{\text{Kleb}} = 0.3, \quad C_{\text{wk}} = 1.0$$

The Cebeci–Smith model has the distinct advantage of being easier to implement while the Baldwin–Lomax model has the advantage of providing a better defined outer length scale. In the present study, both models are used to examine their effectiveness in simulating unsteady turbulent pipe flow.

APPENDIX B: NOMENCLATURE

a	wave speed
D	pipe diameter
g	gravitational acceleration
f	Darcy friction factor

H	pressure head
H_0	pressure head at steady state
L	pipe length
r	radial location across the pipe
R	pipe radius
t	time
u	axial component of velocity
u_τ	friction velocity
v	radial component of velocity
V	average cross-sectional velocity
V_0	average cross-sectional velocity at steady state
x	axial location along the pipe
y	distance from pipe wall ($y = R - r$)
α	numerical switch for detecting regions of high gradients
Δt	time step
Δx	spatial step in axial direction
v	kinematic viscosity
v_t	eddy viscosity
ρ	fluid density
τ	stress tensor
CFL	$a\Delta t/\Delta x$
Re	Reynolds number $= V_o D/v$

REFERENCES

1. Ghidaoui MS, Zhao M, McInnis DA, Axworthy DH. A review of water hammer theory and practice. *ASME Applied Mechanics Reviews* 2005; **58**(1):49–76.
2. Wylie EB, Streeter VL. *Fluid Transients in Systems*. Prentice-Hall: Englewood Cliffs, NJ, 1993.
3. Tan JK, Ng KC, Nathan GK. Application of the centre implicit method for investigation of pressure transients in pipelines. *International Journal for Numerical Methods in Fluids* 1987; **7**(4):395–406.
4. Hwang Y, Chung N. A fast Godunov method for the water-hammer problem. *International Journal for Numerical Methods in Fluids* 2002; **40**(6):799–819.
5. Szymkiewicz R, Mitosek M. Analysis of unsteady pipe flow using the modified finite element method. *Communications in Numerical Methods in Engineering* 2005; **21**(4):183–199.
6. Zielke W. Frequency-dependent friction in transient pipe flow. *Journal of Basic Engineering*, *Transactions of the ASME* 1968; **90**(1):109–115.
7. Brunone B, Golia UM, Greco M. Some remarks on the momentum equation for fast transients. *Proceedings of the International Conference on Hydraulic Transients with Water Column Separation*, IAHR, Valencia, Spain, 1991; 201–209.
8. Brunone B, Golia UM, Greco M. Modeling of fast transients by numerical methods. *Proceedings of the International Conference on Hydraulic Transients with Water Column Separation*, IAHR, Valencia, Spain, 1991; 273–280.
9. Brunone B, Golia UM, Greco M. Effects of two-dimensionality on pipe transients modeling. *Journal of Hydraulic Engineering* 1995; **121**(12):906–912.
10. Vardy AE, Hwang KL, Brown J. A weighting function model of transient turbulent pipe friction. *Journal of Hydraulic Research* 1993; **31**(4):533–548.
11. Vardy AE, Brown J. Transient, turbulent, smooth pipe friction. *Journal of Hydraulic Research* 1995; **33**(4): 435–456.
12. Vardy AE, Brown J. Efficient approximation of unsteady friction weighting functions. *Journal of Hydraulic Engineering* 2004; **130**(11):1097–1107.
13. Bratland O. Frequency-dependent friction and radial kinetic energy variation in transient pipe flow. *Proceedings of the 5th International Conference on Pressure Surges*, British Hydrodynamics Research Association, Cranfield, U.K., 1986; 95–101.

14. Nathan GK, Tan JK, Ng KC. Two-dimensional analysis of pressure transients in pipelines. *International Journal for Numerical Methods in Fluids* 1988; **8**(3):339–349.
15. Vardy AE, Hwang KL. A characteristics model of transient friction in pipes. *Journal of Hydraulic Research* 1991; **29**(5):669–684.
16. Pezzinga G. Quasi-2D model for unsteady flow in pipe networks. *Journal of Hydraulic Engineering* 1999; 676–685.
17. Brunelli MCP. Two-dimensional pipe model for laminar flow. *ASME Journal of Fluids Engineering* 2005; **127**:431–437.
18. Baldwin BS, Lomax H. Thin-layer approximation and algebraic model for separated turbulent flows. *AIAA Paper 78-257* 1978.
19. Smith AMO, Cebeci T. Numerical solution of the turbulent boundary layer equations. *Douglas Aircraft Division Report DAC 33735* 1967.
20. Jameson A, Schmidt W, Turkel E. Numerical solution of the Euler equations by finite volume methods using Runge–kutta time-stepping schemes. *AIAA Paper 81-1259* 1981.
21. Swanson RC, Turkel E. On central difference and upwind schemes. *Journal of Computational Physics* 1992; **101**:292–306.
22. Holmboe EL, Rouleau WT. The effect of viscous shear on transients in liquid lines. *Journal of Basic Engineering*, *Transactions of the ASME* 1967; **89**(1):174–180.
23. Wilcox D. *Turbulence Modeling for CFD* (2nd edn). DCW Industries, 1998.
24. Stokes G. On the effect of the internal friction of fluids on the motion of pendulums. *Transactions of the Cambridge Philosophical Society* 1851; **9**:8–106.
25. Sarpkaya T. On the parameter $\beta = Re/KC = D^2/vT$. *Journal of Fluids and Structures* 2005; **21**(4):435–440.

